LUND UNIVERSITY

Models and methodology for optimal trajectory generation in safety-critical road–vehicle manoeuvres

Berntorp, Karl; Olofsson, Björn; Lundahl, Kristoffer; Nielsen, Lars

Link to publication

RESEARCH ARTICLE

Models and Methodology for Optimal Trajectory Generation in Safety-Critical Road-Vehicle Maneuvers

Karl Berntorp[a*], Björn Olofsson[a], Kristoffer Lundahl[b], and Lars Nielsen[b]

[a]*Department of Automatic Control, Lund University, SE–221 00 Lund, Sweden*
(E-mail: {karl.berntorp, bjorn.olofsson}@control.lth.se)
[b]*Department of Electrical Engineering, Division of Vehicular Systems, Linköping*
University, SE–581 83 Linköping, Sweden
(E-mail: {kristoffer.lundahl, lars.nielsen}@liu.se)

There is currently a strongly growing interest in obtaining optimal control solutions for vehicle maneuvers, both in order to understand optimal vehicle behavior and, perhaps more importantly, to devise improved safety systems, either by direct deployment of the solutions or by including mimicked driving techniques of professional drivers. However, it is nontrivial to find the right combination of models, optimization criteria, and optimization tools to get useful results for the above purposes. Here, a platform for investigation of these aspects is developed based on a state-of-the-art optimization tool together with adoption of existing vehicle chassis and tire models. A minimum-time optimization criterion is chosen to the purpose of gaining insight in at-the-limit maneuvers, with the overall aim of finding improved fundamental principles for future active safety systems. The proposed method to trajectory generation is evaluated in time-critical maneuvers using vehicle models established in literature. We determine the optimal control solutions for three maneuvers, using tire and chassis models of different complexity. The results are extensively analyzed and discussed. Our main conclusion is that the tire model has a fundamental influence on the resulting control inputs. Also, for some combinations of chassis and tire models, inherently different behavior is obtained. However, certain variables important in vehicle safety-systems, such as the yaw moment and the body-slip angle, are similar for several of the considered model configurations in aggressive maneuvering situations.

Keywords: optimal maneuvers; time-optimal trajectory generation; road vehicles; chassis and tire modeling.

1.   Introduction

Optimization of vehicle trajectories can be motivated from different perspectives. One objective is to develop improved active safety systems for standard customer cars. The Electronic Stability Control (ESC) systems, see [1] and [2], of today are still behind the maneuvering performance achievable by professional rally-car drivers in critical situations, but the vision for improvement is there [3]. A recent survey on optimal control in automotive applications [4] points out:

> Most often, the optimal control itself will be interesting mainly insofar as it enables the discovery of the best possible system performance. Occasionally, the optimal control will provide a basis for the design and operation of practical systems.

Further, the survey points out that finding the right balance between models, correct formulations, and optimization methods is the fundamental problem to be solved. Moreover, the survey states that the development today is hampered by long simulation and optimization times. However, we see that with recent increase in computing power and advances in numerical methods for nonlinear optimization, the simulation and optimization times achievable today enable offline investigation of multiple model categories as well as vehicle parameters. The possibilities for online trajectory generation are still not there, mainly because of the inherent nonconvexity of the optimal control problem.

It is a common observation that the criterion of time-optimality in aggressive vehicle maneuvers, combined with input and state constraints, often result in control signals utilizing the achievable limits of the input and state regions. It is therefore crucial how, for example, the tires are modeled outside their normal range of operation. In addition, chassis dynamics such as roll and pitch motion are important to give a correct representation of load transfer and vehicle stability.

The interaction between tire and road is complex, and different tires and roads have different characteristics [5]. Even when only considering the longitudinal stiffness, that is, the initial slope of the longitudinal force-slip curve, the experimental values differ considerably between tires, and the variability can typically be 20–100%, see [6]. Further, in addition to the differences in stiffness there are also deviations between the characteristic shape of the curve at the maximum force, where the peak can be more or less accentuated. This is illustrated for Pacejka's Magic Formula and the Highway Safety Research Institute (HSRI) models in [6]. The complete tire model capturing both longitudinal and lateral forces can thus be expected to have large variability in shape and parameters, and parameter irregularity for different tires. Moreover, the characteristics of the tire forces depend on the road surface [7].

1.1. *Objectives*

The objective of this paper is to utilize recent advances in optimization tools to develop a platform for study of optimal vehicle-maneuvering problems. The purpose is to demonstrate the usefulness of the platform, and to obtain insightful solutions where one specific interest is in future on-board systems for control and safety. Regarding methodology, this means that the control-oriented goal is to find a formulation that gives insight into improved safety systems that benefit from the recent developments in sensor and computing power technology in vehicles; for example, future driver-assistance systems performing closer to what the most experienced drivers can do. To that end we study the time-optimal maneuvers in three different scenarios; a 90°-turn, a hairpin turn (see Figure 1), and a double lane-change maneuver.

As already noted, it is stated in [4] that modeling is a crucial part. Different versions of the well known single-track (ST) and double-track (DT) chassis models have been used in several safety systems and optimal vehicle maneuver studies, see [8–13] for examples with ST and [14, 15] for examples with DT. An ST model sufficiently captures planar dynamics and has the advantage of lower computational complexity because of its reduced number of states. Consequently, it has greater promise for onboard systems. On the other hand, a DT model captures motion in space. In general, however, it requires more computation time when solving

Figure 1. An example of a hairpin turn. Photo courtesy of RallySportLive.

the corresponding optimization problem. It is thus a natural objective to study a spectrum of chassis models and compare both the solutions and the computational burden. With the perspective of future control systems, it is natural to include the control signals, being the drive or brake torques on the wheels. This means that we include wheel dynamics, which is an extension of what many previous studies have done, see, for example, [14–17]. Finally, there is the aspect of modeling of the tire-road interaction. Such models are reproductions of the situation under which they were measured or may be an average over different conditions, and they may exhibit significant differences. Also here, aiming at onboard solutions, it is an objective to investigate a spectrum of tire–road models from simple to more descriptive (but more computationally demanding). One especially important aspect is worth mentioning already here; model behavior and requirements are quite different between simulation and optimization. Even though many models have been used in simulation for many years, and shown good agreement with reality, time-optimal optimization problems tend to result in control inputs corresponding to aggressive maneuvering. The optimal control inputs push the models to, and even beyond, their limits, leading to nonphysical behavior. Another issue is that tire–road models often depend on parameter fit and as such may have properties that can be managed in simulation tools, but may result in convergence to local minima and numerical instability in the optimization, if not properly handled. All these modeling aspects are important. Thus, to demonstrate the value of a platform for study of optimal vehicle-maneuvering problems, it must be verified that the platform provides sensible solutions for a spectrum of models with different characteristics. We have used our platform with several model combinations, and in this paper we present six different combinations of chassis and tire models, all of which are common in literature, and discuss and analyze the results in detail. The chosen model configurations are the ones deemed most interesting for the analysis and understanding of the balance between accuracy and computational demand for future automotive safety systems.

1.2.   *Background*

Optimal control problems for vehicles in time-critical situations have been studied previously, see [8, 12, 18, 19] for different examples concerning T-bone collisions and cornering. The influence of the road surface and the car transmission layout was investigated in [20] using a ST chassis model. Control laws for vehicle emergency-maneuvers were developed in [11] based on an analytical optimal-control approach. However, certain assumptions on the vehicle dynamics were imposed, and roll and

pitch dynamics for the chassis were neglected. Optimal lane-change maneuvers were theoretically investigated in [21]. In particular, the minimum distance at which an approaching obstacle can be avoided was determined, given an initial speed and the optimal feasible maneuver. The time-optimal race-car line was investigated in [22, 23], and in [4] a survey on existing vehicle dynamics applications of optimal control theory was presented. In contrast to the classical optimal control approach to vehicle maneuver optimization, an approximate linearization approach leading to a sequence of convex optimization problems (one problem for each point in a discrete grid along the spatial path of the vehicle) was proposed in [13]. Methods for constraint-based trajectory planning for optimal maneuvers were developed in [24, 25]. In [10], the stability and agility of aggressive pendulum-turn maneuvers, performed by professional race-car drivers, were investigated. Further, [14, 15] discussed optimal control of over-actuated vehicles, where similar optimization tools as those employed in this paper were utilized. A method for optimal control allocation in yaw stabilization of automotive vehicles was proposed in [16], and an expansion of the work comprising a two-level strategy for active steering and adaptive control allocation was presented in [26]. Further, an optimal yaw-control law for road vehicles was discussed in [9].

The authors have previously presented a method for determining optimal maneuvers and a subsequent comparison using different methods for tire modeling in [27], and a comparison of optimal maneuvers with different chassis models was treated in [28]. Moreover, we investigated the influence of the road surface on the optimal maneuver in [29]. Further, in [30] we reported that simplified vehicle models, such as the ST model, identified from experimental data managed to replicate the behavior of real vehicles. However, this was based on less aggressive driving situations, and not using optimization as a criterion for determining the control inputs.

1.3.   *Relation to Previous Work and Outline*

A preliminary version of parts of the research presented here has been presented as conference contributions [27, 28]. In this paper, several extensions are presented. In particular, regarding methodology, more combinations of chassis and tires models of various complexity are investigated, and a more efficient and robust initialization procedure to the time-optimal optimization problem is proposed. In addition, an extensive comparison of the obtained results and a more in-depth analysis for the different maneuvers are provided.

The rest of this paper is outlined as follows: The problem formulation and specific aim of the paper are discussed in Section 2. Vehicle and tire modeling and the specific models investigated here are presented in Section 3, followed by the formulation and solution method for the studied time-optimal maneuvering problem in Section 4. Optimization results and a subsequent analysis of the obtained results are provided in Section 5. The proposed method to trajectory optimization and the significance of the obtained results are discussed in Section 6, where conclusions also are drawn.

2.   Problem Formulation

The goal of the research presented in this paper is twofold. The first goal is control-oriented and consists of finding the time-optimal vehicle trajectory when maneuvering through a time-critical situation, with the vehicle being subject to various

constraints, which are motivated by physical limitations of the driver and the vehicle and the road geometry.

The second goal is model oriented and aims at investigating whether different chassis and tire models yield fundamentally different solutions, not only in the cost function in the optimization but also in the internal vehicle behavior. Of particular interest is to analyze the results from a safety-system perspective; that is, what driving behavior and model characteristics can be extracted from the results. Hence, a part of the research is devoted to investigating how the models differ. We consider differential-algebraic equation (DAE) models of the form

$$\dot{x}(t) = G(x(t), y(t), u(t)),$$
$$0 = h(x(t), y(t), u(t)),$$

where $G(x(t), y(t), u(t))$ and $h(x(t), y(t), u(t))$ are twice continuously differentiable nonlinear functions of the vehicle differential variables x, algebraic variables y, and control inputs u, where the time-dependency of the variables will be implicit in the rest of the paper. The employed vehicle models differ in both chassis and tire aspects. We assume that the tires stay in contact with the ground at all times. This is usually not a severe restriction for the average passenger vehicle under normal operating conditions. However, considering high-performance vehicle configurations in tight cornering, this modeling aspect would need further elaboration. The complete formulation of the optimal control problem is given in Section 4, and results in a general framework well suited for the studies performed.

3. Modeling

The vehicle dynamics modeling presented in this section incorporates the chassis motion modeling (having a varying number of degrees of freedom) and the tire force modeling. Further, we discuss calibration of the tire models and present a subsequent investigation of the qualitative behavior of the studied tire models.

3.1. *Chassis Models*

We use three chassis models of different complexity. The most complex model is a DT model with roll (ϕ) and pitch (θ) dynamics and both longitudinal and lateral load transfer[1]. This chassis model is illustrated in Figure 2. The model has five degrees of freedom, namely two translational and three rotational. The chassis rotational motions in the roll, pitch, and yaw directions are characterized by the vehicle chassis inertias I_{xx}, I_{yy}, and I_{zz}, respectively. The derivation of the double-track model is omitted because of space limitations; for the details we refer to [31, 32]. We will, however, state the equations for the complete model in what follows.

3.1.1. *DT Model*

The suspension system is modeled as a rotational spring-damper system. Consequently, the moment τ_ϕ produced by the suspension system in the roll direction is

---

[1]Motivated by a passenger vehicle perspective in the analysis, we neglect aerodynamic modeling in the chassis dynamics. It can, however, easily be introduced in the proposed modeling framework if rally or racing applications are to be investigated.

given by

$$\tau_\phi = (K_{\phi,f} + K_{\phi,r})\phi + (D_{\phi,f} + D_{\phi,r})\dot{\phi}, \tag{1}$$

and correspondingly for the moment τ_θ in the pitch direction according to

$$\tau_\theta = K_\theta \theta + D_\theta \dot{\theta}, \tag{2}$$

where K and D are parameters. Throughout the paper we use the indices f, r and $1, 2, 3, 4$ for denoting the respective wheel pair and wheel, respectively. The dynamic equations for the longitudinal load transfer are given by

$$(F_{z,1} + F_{z,2})l_f - (F_{z,3} + F_{z,4})l_r = K_\theta \theta + D_\theta \dot{\theta}, \quad \sum_{i=1}^{4} F_{z,i} = mg \tag{3}$$

where $F_{z,i}$, $i \in \{1, 2, 3, 4\}$, denote the time-dependent normal forces, m is the vehicle mass, l_f, l_r are defined in Figure 2, and g is the constant of gravity. The lateral load transfer is determined by the relations

$$-w(F_{z,1} - F_{z,2}) = K_{\phi,f}\phi + D_{\phi,f}\dot{\phi}, \tag{4}$$

$$-w(F_{z,3} - F_{z,4}) = K_{\phi,r}\phi + D_{\phi,r}\dot{\phi}, \tag{5}$$

where w is defined in Figure 2.

The translational dynamic equations, which are straightforward to derive using a Newton-Euler approach, are given by

$$\dot{v}_x - v_y\dot{\psi} = h\Big(\sin(\theta)\cos(\phi)(\dot{\psi}^2 + \dot{\phi}^2 + \dot{\theta}^2) - \sin(\phi)\ddot{\psi} - 2\cos(\phi)\dot{\phi}\dot{\psi}$$

$$- \cos(\theta)\cos(\phi)\ddot{\theta} + 2\cos(\theta)\sin(\phi)\dot{\theta}\dot{\phi} + \sin(\theta)\sin(\phi)\ddot{\phi}\Big) + \frac{F_X}{m}$$

$$\dot{v}_y + v_x\dot{\psi} = h\Big(-\sin(\theta)\cos(\phi)\ddot{\psi} - \sin(\phi)\dot{\psi}^2 - 2\cos(\theta)\cos(\phi)\dot{\theta}\dot{\psi}$$

$$+ \sin(\theta)\sin(\phi)\dot{\phi}\dot{\psi} - \sin(\phi)\dot{\phi}^2 + \cos(\phi)\ddot{\phi}\Big) + \frac{F_Y}{m},$$

where v_x, v_y are the longitudinal and lateral velocities at the mass center, $\dot{\psi}$ is the yaw rate, and h is the distance from the roll center to the mass center. Moreover,

$$F_X = F_{x,1}\cos(\delta) - F_{y,1}\sin(\delta) + F_{x,2}\cos(\delta) - F_{y,2}\sin(\delta) + F_{x,3} + F_{x,4}, \tag{6}$$

$$F_Y = F_{x,1}\sin(\delta) + F_{y,1}\cos(\delta) + F_{x,2}\sin(\delta) + F_{y,2}\cos(\delta) + F_{y,3} + F_{y,4}, \tag{7}$$

where δ is the steer angle, $F_{x,i}$ is the longitudinal force for wheel i, and similarly for the lateral direction. The rotational dynamic equation for ψ is given by

$$\ddot{\psi}(I_{xx}\sin(\theta)^2 + \cos(\theta)^2(I_{yy}\sin(\phi)^2 + I_{zz}\cos(\phi)^2)) = M_Z - h\Big(F_X\sin(\phi)$$

$$+ F_Y\sin(\theta)\cos(\phi)\Big), \tag{8}$$

where

$$M_Z = l_f \Big(F_{x,1} \sin(\delta) + F_{x,2} \sin(\delta) + F_{y,1} \cos(\delta) + F_{y,2} \cos(\delta) \Big)$$
$$+ w_f \Big(-F_{x,1} \cos(\delta) + F_{x,2} \cos(\delta) + F_{y,1} \sin(\delta) - F_{y,2} \sin(\delta) \Big)$$
$$- l_r(F_{y,3} + F_{y,4}) - w_r(F_{x,3} + F_{x,4}). \quad (9)$$

Note that because of the deflection of the center of mass, the external forces in the x- and y-directions give rise to additional external torques τ_z, in this case

$$\tau_z = -h(F_X \sin(\phi) + F_Y \sin(\theta) \cos(\phi)).$$

The pitch dynamics are written as

$$\ddot{\theta}(I_{yy} \cos(\phi)^2 + I_{zz} \sin(\phi)^2) = -K_\theta \theta - D_\theta \dot{\theta}$$
$$+ h\Big(mg \sin(\theta) \cos(\phi) - F_X \cos(\theta) \cos(\phi) \Big) + \dot{\psi}\Big(\dot{\psi} \sin(\theta) \cos(\theta)(\Delta I_{xy}$$
$$+ \cos(\phi)^2 \Delta I_{yz}) - \dot{\phi}(\cos(\theta)^2 I_{xx} + \sin(\phi)^2 \sin(\theta)^2 I_{yy}$$
$$+ \sin(\theta)^2 \cos(\phi)^2 I_{zz}) - \dot{\theta}\Big(\sin(\theta) \sin(\phi) \cos(\phi)\Delta I_{yz} \Big) \Big), \quad (10)$$

where $\Delta I_{xy} = I_{xx} - I_{yy}$ and $\Delta I_{yz} = I_{yy} - I_{zz}$. Using $K_\phi = K_{\phi,f} + K_{\phi,r}$ and $D_\phi = D_{\phi,f} + D_{\phi,r}$, the third equation of angular motion equals

$$\ddot{\phi}(I_{xx} \cos(\theta)^2 + I_{yy} \sin(\theta)^2 \sin(\phi)^2 + I_{zz} \sin(\theta)^2 \cos(\phi)^2) = -K_\phi \phi - D_\phi \dot{\phi}$$
$$+ h(F_Y \cos(\phi) \cos(\theta) + mg \sin(\phi))$$
$$+ \dot{\psi}\Delta I_{yz}\Big(\dot{\psi} \sin(\phi) \cos(\phi) \cos(\theta) + \dot{\phi} \sin(\theta) \sin(\phi) \cos(\phi) \Big)$$
$$+ \dot{\psi}\dot{\theta}(\cos(\phi)^2 I_{yy} + \sin(\phi)^2 I_{zz}). \quad (11)$$

3.1.2. ST-pitch Model

The second model is a single-track model, where we have added pitch dynamics (ST-pitch). The dynamics incorporate the same modeling of the suspension system in the pitch direction as for the DT model. The dynamic equations for this model are conceptually found from DT by lumping the left and right wheel on each axle together and setting the roll angle to zero. This results in the following equations of motion in the translational directions

$$\dot{v}_x - v_y\dot{\psi} = h(\sin(\theta)(\dot{\psi}^2 + \dot{\theta}^2) - \cos(\theta)\ddot{\theta}) + \frac{F_X}{m},$$
$$\dot{v}_y + v_x\dot{\psi} = -h(\sin(\theta)\ddot{\psi} + 2\cos(\theta)\dot{\theta}\dot{\psi}) + \frac{F_Y}{m},$$

and the following in the rotational directions

$$(I_{zz} + I_{xx} \sin(\theta)^2)\ddot{\psi} = M_Z - h\sin(\theta)F_Y,$$
$$\ddot{\theta}I_{yy} + D_\theta\dot{\theta} + K_\theta\theta - mgh\sin(\theta) = -h\cos(\theta)F_X + \dot{\psi}^2 \sin(\theta)\cos(\theta)\Delta I_{xz},$$
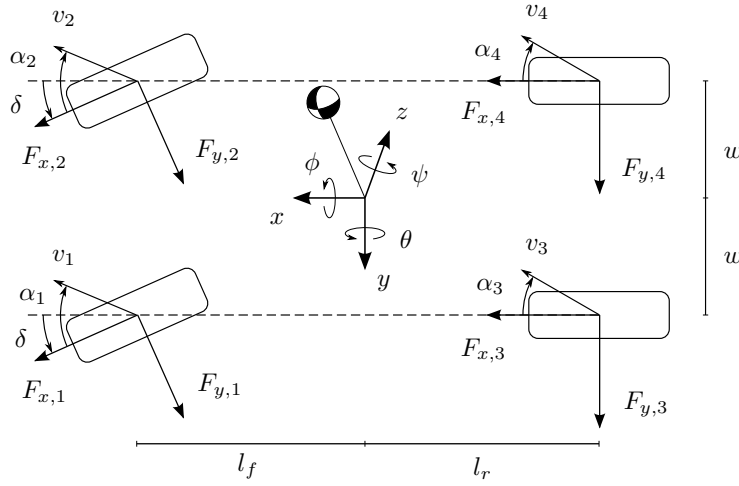
Figure 2. The double-track model, with roll and pitch dynamics. Note that the geometric lateral slip angle is shown in the figure.
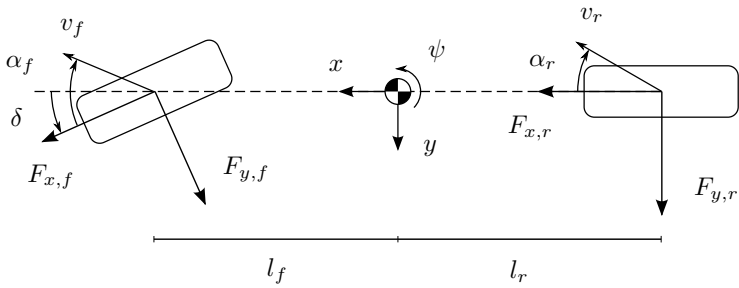
Figure 3. The single-track model. Note that the geometric lateral slip angle is shown in the figure.

where $\Delta I_{xz} = I_{xx} - I_{zz}$ and F_X, F_Y, and M_Z are the lumped total forces, as opposed to (6), (7), and (9). The load transfer equations in the pitch direction are given by (3), where the wheel forces on each axle are lumped together for the ST-pitch chassis model.

3.1.3. ST Model

The third model is a single-track model (ST), illustrated in Figure 3. This model lumps together the left and right wheel on each axle, and roll and pitch dynamics are neglected. Thus, the model has two translational and one rotational degrees of freedom. The model dynamics are straightforward to derive [33] and are given by

$$\dot{v}_x - v_y\dot{\psi} = \frac{1}{m}(F_{x,f}\cos(\delta) + F_{x,r} - F_{y,f}\sin(\delta)) = \frac{F_X}{m}, \tag{12}$$

$$\dot{v}_y + v_x\dot{\psi} = \frac{1}{m}(F_{y,f}\cos(\delta) + F_{y,r} + F_{x,f}\sin(\delta)) = \frac{F_Y}{m}, \tag{13}$$

$$I_{zz}\ddot{\psi} = l_f F_{y,f}\cos(\delta) - l_r F_{y,r} + l_f F_{x,f}\sin(\delta) = M_Z, \tag{14}$$

where F_X, F_Y, and M_Z are the global forces. The nominal normal force F_{z0} resting on the respective wheel in steady state is given by

$$F_{z0,f} = mg\frac{l_r}{l}, \quad F_{z0,r} = mg\frac{l_f}{l}, \tag{15}$$

where the wheel base is defined as $l = l_f + l_r$.

3.2. *Wheel and Tire Modeling*

The slip angles α_i and slip ratios κ_i are defined as in [5]:

$$\dot{\alpha}_i \frac{\sigma}{v_{x,i}} + \alpha_i = -\arctan\left(\frac{v_{y,i}}{v_{x,i}}\right), \tag{16}$$

$$\kappa_i = \frac{R_w \omega_i - v_{x,i}}{v_{x,i}}, \ \ i \in \{f,r\} \text{ or } \{1,2,3,4\}, \tag{17}$$

where σ is the relaxation length, R_w is the wheel radius, ω_i is the wheel angular velocity for wheel i, and $v_{x,i}$ and $v_{y,i}$ are the longitudinal and lateral wheel velocities for wheel i with respect to an inertial system, expressed in the coordinate system of the wheel. The wheel dynamics[1], necessary for slip-ratio computation, are given by

$$T_i - I_w \dot{\omega}_i - F_{x,i} R_w = 0 \ , \quad i \in \{f,r\} \text{ or } \{1,2,3,4\}. \tag{18}$$

Here, T_i is the driving/braking torque and I_w is the wheel inertia.

When developing a platform for investigation of optimal maneuvers, it is of interest to handle and compare different tire characteristics, and thus to cope with different tire models. The nominal tire forces F_{x0} and F_{y0}—that is, the forces under pure slip conditions—are computed with the Magic Formula model [5], given by

$$F_{x0,i} = \mu_{x,i} F_{z,i} \sin(C_{x,i}\arctan(B_{x,i}\kappa_i - E_{x,i}(B_{x,i}\kappa_i - \arctan B_{x,i}\kappa_i))), \tag{19}$$

$$F_{y0,i} = \mu_{y,i} F_{z,i} \sin(C_{y,i}\arctan(B_{y,i}\alpha_i - E_{y,i}(B_{y,i}\alpha_i - \arctan B_{y,i}\alpha_i))), \tag{20}$$

for each wheel $i \in \{f,r\}$ or $\{1,2,3,4\}$. In (19)–(20), μ_x and μ_y are the friction coefficients and B, C, and E are model parameters.

Under combined slip conditions—that is, both κ and α are nonzero—the longitudinal and lateral tire forces will depend on both slip quantities. How this coupling is described can have immense effect on the vehicle dynamics. In an optimal maneuver, the computed control inputs will result in the best combination of longitudinal and lateral force, and these forces are, of course, coupled via the physics of the tire. Even though detailed experiments, like the ones in [6] for longitudinal stiffness, are lacking for the complete longitudinal-lateral tire interaction, there is a vast plethora of characteristics, see [1], [5], [34], and [35]. We have chosen two different tire model categories for our study, which are described next.

3.2.1. *Combined Forces based on the Friction Ellipse*

A straightforward model of combined forces is based on the friction ellipse, and is described by the elliptical constraint

$$F_{y,i} = F_{y0,i}\sqrt{1 - \left(\frac{F_{x0,i}}{\mu_{x,i}F_{z,i}}\right)^2}, \ \ i \in \{f,r\} \text{ or } \{1,2,3,4\}, \tag{21}$$

where F_{x0} is used as an input variable, see for example [36]. However, we have opted for using the driving/braking torques as input, see (18), since this is a quantity

---

[1]In the wheel dynamic modeling, we assume that the vehicle has an open differential, motivated by a passenger-vehicle perspective in the study. However, we have verified that the proposed optimization framework can handle other differential settings, such as locking differential on the rear axle and limited-slip differential, as well.

that can be controlled in a physical setup of a vehicle. The main limitation with the friction ellipse model is that the longitudinal force does not explicitly depend on the lateral slip, which is not realistic. With longitudinal slip present, it is possible to use a related, more involved model, which is also based on the friction ellipse [34]. However, we use (21) because it represents the simplest combined-force model that is used in the vehicle optimal-control literature [14, 15]. This model will hereafter be denoted the friction ellipse (FE) model.

3.2.2.   *Representing Combined Slip with Weighting Functions*

Another more comprehensive approach to tire modeling, which is inspired by the Magic Formula and explicitly accounting for the effect on the tire force by the longitudinal and lateral slip, is to scale the nominal forces (19)–(20) with weighting functions $G_{x\alpha,i}$ and $G_{y\kappa,i}$, which depend on α and κ [5]. The relations in the longitudinal direction are

$$H_{x\alpha,i} = B_{x1,i} \cos(\arctan(B_{x2,i}\kappa_i)), \tag{22}$$

$$G_{x\alpha,i} = \cos(C_{x\alpha,i} \arctan(H_{x\alpha,i}\alpha_i)), \tag{23}$$

$$F_{x,i} = F_{x0,i}G_{x\alpha,i}, \ i \in \{f,r\} \text{ or } \{1,2,3,4\}, \tag{24}$$

and the corresponding relations in the lateral direction are given by

$$H_{y\kappa,i} = B_{y1,i} \cos(\arctan(B_{y2,i}\alpha_i)), \tag{25}$$

$$G_{y\kappa,i} = \cos(C_{y\kappa,i} \arctan(H_{y\kappa,i}\kappa_i)), \tag{26}$$

$$F_{y,i} = F_{y0,i}G_{y\kappa,i}, \ i \in \{f,r\} \text{ or } \{1,2,3,4\}, \tag{27}$$

where B and C are model parameters. Throughout the paper, (22)–(27) will be denoted the weighting functions (WF) model.

3.3.   *Calibrating Tire Models for Comparison*

When comparing an optimal maneuver based on two different tire models, it is not obvious how to calibrate the models with respect to the specific tire to get comparable solutions to the optimal control problem. As an example, Figure 4 shows the resulting tire forces for two tire models; the first is parametrized using FE and the second is parametrized using WF. To equalize these models in comparative studies, one way would be to have the same average resultant force, whereas another way would be to equalize the longitudinal stiffness. For the particular tire models considered in this study, the same parameters have been used in the relations for the nominal longitudinal and lateral forces in (19)–(20), that is, for pure slip conditions the two tire models agree. In the calibration procedure, we neglect that parts of the tire model parameters depend on the time-varying normal force; instead the parameters are determined from the normal forces present when the vehicle is in steady state.

3.3.1.   *Qualitative Behavior of Tire Models*

We use the force–slip tire characteristic surfaces as a basis for analysis, as introduced in [27] and hereafter referred to as Force-Slip (FS)-diagrams. This 3D

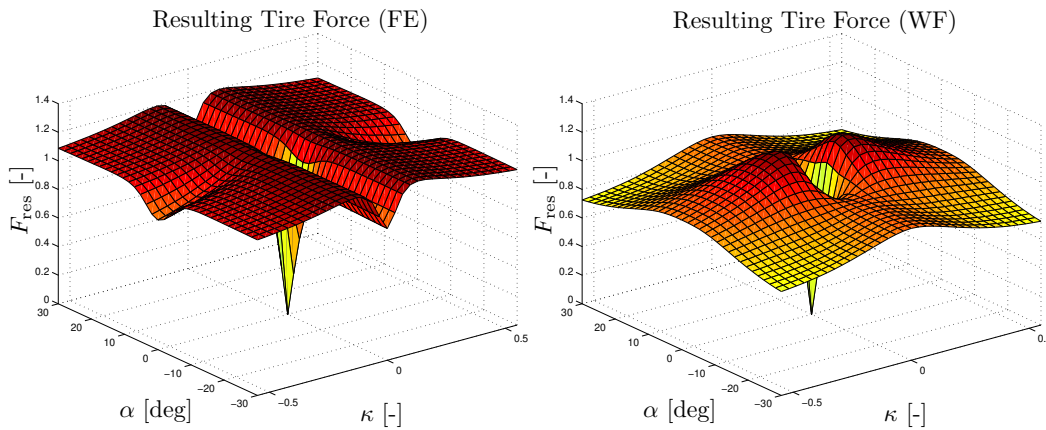Resulting Tire Force (FE)   Resulting Tire Force (WF)

Figure 4.   Resultant tire force F_{res} for the front wheel with a friction ellipse model (left) and a weighting functions model (right), with experimental parameters from [5] according to Table 3. The force is normalized with the steady-state load.

surface is defined as the resulting force

$$F_{\text{res},i} = \frac{\sqrt{(F_{x,i})^2 + (F_{y,i})^2}}{F_{z,i}}, \ i \in \{f,r\} \text{ or } \{1,2,3,4\}, \tag{28}$$

as function of the longitudinal slip κ and slip angle α. The resultant is normalized with the normal force in order to enable comparison of models with and without dynamic load transfer. The model based on the weighting functions is parametrized according to parameters found from experiments in [5], representing a tire behavior when driving on dry asphalt. The friction ellipse model also uses the parameters in [5] for the nominal tire forces. Figure 4 shows how the resulting tire force for the front wheel varies over slip angle and slip ratio for the friction ellipse and the weighting functions models with the parameters presented in Table 3. Studying Figure 4 gives a basis for discussion of the behavior of the tire models in an optimal maneuver; for example, the models give different force characteristics for combined slip, where the most prominent difference is that FE predicts a significantly larger force for combined slip of high values than WF does. Further, the characteristic peaks in F_{res} obviously influence the behavior of the tire force model significantly.

Another fundamental difference between the models is seen in Figure 5, where the lateral force is plotted against the longitudinal force for FE and WF. Differences between the two approaches are clear. In particular, the longitudinal force increases monotonically with decreasing lateral force for FE, which is not the case for WF. Typically, experimental results exhibit similar behavior as WF.

4.   Optimal Control Problem

Based on the chassis and tire dynamics described in Section 3, the time-optimal solutions for different maneuvering situations are to be determined. These trajectories are computed as the solution to an optimization problem and considering the physical setup of the problem, it is clear that a solution exists given that the initial velocity of the vehicle is chosen appropriately. The resulting optimization problems are more challenging than thought at first sight, since the time-optimality implies that the tire-friction models operate on the boundary of their validity. Also, solving dynamic optimization problems numerically where the time horizon is free is in general more demanding than solving a problem with fixed time horizon, because it adds additional degrees of freedom. Further, we have found that nu-

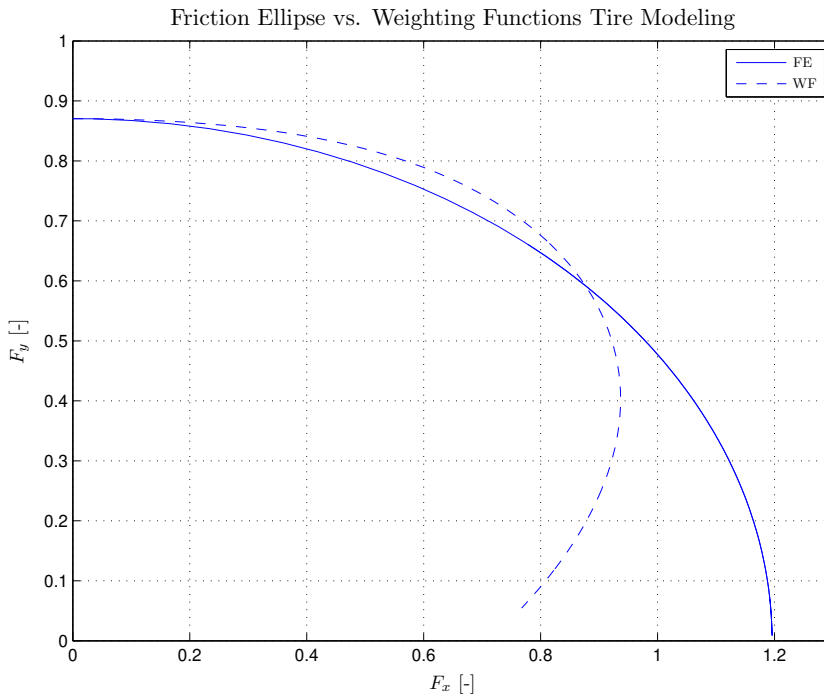Friction Ellipse vs. Weighting Functions Tire Modeling

Figure 5.   Lateral force plotted versus longitudinal force (normalized) for the friction ellipse (FE) and weighting functions (WF) models, respectively, for $\alpha = 7.6°$, $\kappa \in [0, 1]$. The models predict different behavior for large values of the longitudinal force; in particular, the longitudinal force increases monotonically with decreasing lateral force for FE. Experimental results tend to support the behavior of WF.

merical issues easily arise and that the optimization does not converge without proper initialization of the model trajectories prior to the optimization. To this purpose, an initialization procedure based on driver models has been developed as part of the optimization platform, see Section 4.3. Moreover, scaling of the optimization variables to the same nominal interval (based on a priori assumptions on their maximum values) is essential in order to avoid ill-conditioned matrices in the optimization procedure.

4.1. *Formulation of the Optimal Control Problem*

The chassis motion models presented are formulated as differential-algebraic equation systems according to $\dot{x} = G(x, y, u)$, as described in Section 2. The wheel driving and braking torques $T = \begin{pmatrix} T_f & T_r \end{pmatrix}$, as well as the steer angle δ of the front wheels are considered as inputs. For simplicity we assume that the front wheels have the same steer angle in the double-track models. Moreover, considering that the analysis in this paper has a focus on optimal maneuvers for passenger vehicles in safety-critical situations, it is justified to assume that the double-track models have one wheel-torque input for each axle. The inputs are equally distributed between the wheels at the respective axle—that is, $T_1 = T_2 = T_f/2$ and $T_3 = T_4 = T_r/2$. This is equivalent to separate front and rear braking systems (where, for example, anti-lock braking systems are disregarded to allow for solutions with large slip), and an open differential. Further, the tire-force model is written as the equation system $h(x, y, u) = 0$. The optimization problem is formulated over the time horizon $t \in [0, t_f]$ and the objective of the optimization is to minimize the final time t_f of the maneuver. Accordingly, the dynamic optimization problem to be solved

is stated as follows:

$$
\begin{aligned}
\text{minimize} \quad & t_f \\
\text{subject to} \quad & T_{i,\min} \leq T_i \leq T_{i,\max}, \ \ i \in \{f, r\} \text{ or } \{1, 2, 3, 4\} \\
& |\dot{T}_i| \leq \dot{T}_{i,\max}, \ \ i \in \{f, r\} \\
& |\delta| \leq \delta_{\max}, \quad |\dot{\delta}| \leq \dot{\delta}_{\max} \\
& x(0) = x_0, \quad x(t_f) = x_{t_f}, \\
& f(X_p, Y_p) \leq 0 \\
& \dot{x} = G(x, y, u), \quad h(x, y, u) = 0
\end{aligned}
\tag{29}
$$

where x_0 are the initial conditions for the differential variables, x_{t_f} are the desired values for the differential variables at the final time $t = t_f$, and (X_p, Y_p) is the position of the center-of-gravity of the vehicle. In practice, the conditions at $t = t_f$ are only applied to a subset of the model state variables. Further, $f(X_p, Y_p)$ is a mathematical description of the road constraint for the center-of-gravity of the vehicle for the respective maneuver. These constraints in the geometric two-dimensional XY-plane are formulated as super-ellipses with different radii and degrees.

4.2.   *Implementation and Solution*

The chassis and tire dynamics were implemented using the modeling language Modelica [37]. Utilizing Optimica [38], which is an extension of Modelica for high-level description of optimization problems based on Modelica models, the implementation of the vehicle and tire dynamics described in Section 3 and the optimal control problem (29) was straightforward.

Because of the complex nature of the nonlinear and nonconvex optimization problem (29), analytical solutions were intractable. Instead, we utilized numerical methods based on simultaneous collocation [39] of the continuous-time problem (29). Simultaneous collocation means that the continuous-time differential, algebraic, and control variables are discretized using an equidistant grid of the time horizon $[0, t_f]$ with N_e elements. In each element $[t_{i-1}, t_i]$, $i = 1, \ldots, N_e$, the optimization variables are approximated using polynomials p of the format

$$
p(t) = \sum_{j=1}^{N_p} p_{i,j} L_j \left(\frac{t - t_{i-1}}{h_p} \right), \quad t \in [t_{i-1}, t_i],
\tag{30}
$$

where $p_{i,j}$ is the interpolation coefficient, L_j is the interpolation polynomial, and h_p is the element length. Moreover, N_p collocation points are chosen in each element; in our implementation these were chosen as the corresponding Radau points. In the particular scheme employed, the differential variables were described using Lagrange polynomials of order N_c, whereas the algebraic and control variables are described using Lagrange polynomials of order $N_c - 1$. In addition, continuity of the differential variables were enforced at the element boundaries with explicit constraints in the optimization. The collocation procedure results in a discrete-time nonlinear program (NLP), where the interpolation coefficients of the polynomials are the optimization variables. For further details on the collocation procedure, see [40]. The resulting NLP is solved using Ipopt [41], which is a numerical solver based on a primal-dual interior-point method opted for large and sparse optimization

problems. The collocation procedure and solution of the optimization problem were performed using the open-source software platform JModelica.org [42, 43]. For the optimization problems considered in this paper, $N_e = 150$ discretization elements were used and each element contained $N_c = 3$ collocation points. The selection of discretization parameters were based on an iterative procedure. The Jacobian and the Hessian related to the problem were required in the Newton iterations in the optimization procedure. Considering the complexity of the employed chassis and tire models, finite-difference approximations of these quantities in quasi-Newton methods such as the Broyden-Fletcher-Goldfarb-Shanno (BFGS) algorithm [44] are not numerically stable, especially not for the DT model. Instead, calculation of the required derivatives with numerical precision (that is, in the order of 10^{-16}) was performed using automatic differentiation [45]; this procedure reduced convergence times several orders of magnitudes and increased numerical stability as compared with the approach using approximate derivatives.

4.3.   *Initialization Procedure*

Robust convergence to a solution of the NLP in Ipopt relies on proper initialization. We have chosen to use simulation of a driver model in combination with the vehicle model to obtain initial trajectories for the model variables in the optimization. The driver model is designed such that the vehicle tracks the middle of the road while following a predefined velocity profile. The driver model, operating the steer angle δ and the rear-wheel torque T_r, is based on a lane-keeping controller described in [35]:

$$\delta = \delta_{ss} - k_1 e - k_2 \dot{e} - k_3 \xi - k_4 \dot{\xi}, \tag{31}$$

$$T_r = T_{r,ff} - k_5(v - v_{\text{nom}}) \tag{32}$$

where δ_{ss} is the steady-state steer angle, e is the lateral deviation from the desired path, ξ is the angular deviation from the desired heading direction, $T_{r,ff}$ is the feedforward term for the rear torque input, v_{nom} is the desired velocity profile, and $\{k_i\}_{i=1}^5$ are driver-model parameters. The controller parameters k_1–k_4 are chosen such that the eigenvalues of the closed-loop system are placed in the same manner as suggested in [35]. The desired velocity v_{nom} is tracked by controlling the rear wheel torques with the feedforward part $T_{r,ff}$, computed from $\dot{v}_{\text{nom}}$, and a term proportional to the speed-profile error.

The authors' experience is that the convergence time is drastically reduced when compared with the approach we utilized in [27], which was based on an iterative optimization procedure with a sequence of smaller subproblems. Using the proposed initialization scheme and a standard PC with an Intel Core i7 CPU in an implementation using only one of the cores, the solution times and number of iterations reported in Table 1 were obtained for the hairpin maneuver, which is the most challenging maneuver considered. Obviously, the number of iterations and computation times are dependent on the complexity of the model configuration and the maneuver; noticeable is that the DT chassis model requires approximately one order of magnitude longer solution time than the ST chassis model.

5.   Results

In this section we present the results achieved by solving the optimal control problem (29) for different vehicle-model configurations in the different maneuver situ-

Table 1. Solution times and number of iterations required for solving the time-optimal maneuver problem in the hairpin turn for the considered model configurations.

Model	Solution Time [s]	No. of Iterations
ST FE	8.0	111
ST WF	12.3	101
ST-pitch FE	16.9	110
ST-pitch WF	7.8	78
DT FE	137.8	340
DT WF	144.2	287

Table 2. Vehicle model parameters used in (1)–(18) for the results presented in this study.

Notation	Value	Unit
l_f	1.3	m
l_r	1.5	m
w	0.8	m
m	2 100	kg
I_{xx}	765	kgm^2
I_{yy}	3 477	kgm^2
I_{zz}	3 900	kgm^2
R_w	0.3	m
I_w	4.0	kgm^2
σ	0.3	m
g	9.82	ms^{-2}
h	0.5	m
$K_{\phi,f}, K_{\phi,r}$	89 000	$\mathrm{Nm(rad)}^{-1}$
$D_{\phi,f}, D_{\phi,r}$	8 000	$\mathrm{Nms(rad)}^{-1}$
K_θ	363 540	$\mathrm{Nm(rad)}^{-1}$
D_θ	30 960	$\mathrm{Nms(rad)}^{-1}$

ations. For each investigated maneuver, the following chassis and tire model configurations were evaluated:

- ST with FE for tire modeling; that is, the single-track model without pitch and roll dynamics, and the friction ellipse for tire modeling.
- ST with WF for tire modeling; that is, the single-track model without pitch and roll dynamics, and the weighting functions for tire modeling.
- ST-pitch with FE for tire modeling; that is, the single-track model with pitch dynamics, and the friction ellipse for tire modeling.
- ST-pitch with WF for tire modeling; that is, the single-track model with pitch dynamics, and the weighting functions for tire modeling.
- DT with FE for tire modeling; that is, the double-track model with pitch and roll dynamics, and the friction ellipse for tire modeling.
- DT with WF for tire modeling; that is, the double-track model with pitch and roll dynamics, and the weighting functions for tire modeling.

The numerical values for the vehicle-model parameters used in this study are provided in Table 2. The corresponding parameters for the tire-force models are found in Table 3.

Table 3.   Model parameters in (19)–(27) used in this study (originating from [5]). The models represent the tire forces on dry asphalt with friction ellipse (FE) and weighting functions (WF), respectively. For DT, the same parameters are used for both the left and the right wheels.

WF	Front	Rear
μ_x	1.20	1.20
B_x	11.7	11.1
C_x	1.69	1.69
E_x	0.377	0.362
μ_y	0.935	0.961
B_y	8.86	9.30
C_y	1.19	1.19
E_y	−1.21	−1.11
B_{x1}	12.4	12.4
B_{x2}	−10.8	−10.8
$C_{x\alpha}$	1.09	1.09
B_{y1}	6.46	6.46
B_{y2}	4.20	4.20
$C_{y\kappa}$	1.08	1.08

FE	Front	Rear
μ_x	1.20	1.20
B_x	11.7	11.1
C_x	1.69	1.69
E_x	0.377	0.362
μ_y	0.935	0.961
B_y	8.86	9.30
C_y	1.19	1.19
E_y	−1.21	−1.11

5.1. *Maneuvers*

Three time-critical maneuvers were chosen for evaluation of the proposed approach to trajectory generation. The motivation for choosing multiple maneuvers is firstly to verify that the developed platform can handle different situations and vehicle behavior, and secondly to enable comparison of the resulting solution for the considered model configurations. The first maneuver is a 90°-turn, which is important in, for example, evaluation of ESC systems in lane-keeping scenarios. The second maneuver is a hairpin turn, which is selected because of its extremity and that it tests several aspects of the tire and chassis modeling. The third maneuver is a double lane-change maneuver, where the dimensions of the track was chosen congruent to the ISO standard 3888-2 [46]. This maneuver is, in particular, common for testing the possibilities for collision avoidance if obstacles are approaching the road, but is also important for evaluation of the roll stability of a vehicle.

5.2. *Optimization Prerequisites*

For the evaluations we set the maximum allowed wheel angle $\delta_{\max}$ and wheel-angle change rate $\dot{\delta}_{\max}$ to 30 deg and 60 deg/s, respectively, which are reasonable parameters, both seen from physical and driver limitations. For all considered maneuvers, the start $(X_{p,0}, Y_{p,0})$ and final vehicle position (X_{p,t_f}, Y_{p,t_f}) were set to be in the middle of the road. The initial velocities were $v_0 = 70$ km/h in the 90°-turn maneuver, $v_0 = 25$ km/h in the hairpin-turn maneuver, and $v_0 = 80$ km/h in the double lane-change maneuver. Further, the lower and upper constraints on the torque inputs were chosen as

$$T_{i,\min} = -\mu_{x,i} R_w mg, \ i \in \{f, r\} \text{ or } \{1, 2, 3, 4\}, \tag{33}$$

$$T_{r,\max} = \mu_{x,r} R_w F_{z0,r}, \tag{34}$$

$$T_{f,\max} = 0, \tag{35}$$

which implies a rear-wheel driven vehicle. The constraints on the derivative of the torque inputs were chosen as $\dot{T}_{i,\max} = 2.5\mu_{x,i} R_w mg, \ i \in \{f, r\}$. Note that the fric-

tion coefficients and the other tire-model parameters on the left and right wheels on the respective axle are assumed to be equal in the DT models. The choice of torque limitations originates from that the maximum braking torques that can be applied on the wheels are significantly larger than the corresponding acceleration torques. Further, the driving torque limit was set to prevent excessive wheel spin, corresponding to large slip ratios. This is motivated since the employed empirical tire models are based on tire-force measurements that for experimental reasons are only possible to obtain for a limited area in the α-κ plane. The reasoning behind having constraints on the derivatives of the input torques is that the driver cannot change the acceleration or deceleration instantly, and in addition the engine or motor time constant limits the change rate of the torque in a physical vehicle. Note, however, that the choice of limitations in this paper is less restrictive than the typical values measured for a combustion engine. Moreover, the wheel velocities were limited to be nonnegative, since solutions with wheel backspin were not desired. Similarly, to aid the solver the longitudinal forces were constrained to $|F_x| \le \mu_x F_z$ and correspondingly for the lateral forces. Note that both the force and wheel-velocity constraints are mathematically redundant.

The analysis of the achieved results presented in this section is focused on the 90°-turn and the hairpin-turn maneuvers. The results from the double lane-change maneuver are commented on and compared to the results obtained for the two other maneuvers in the discussion in Section 6.

5.3.   *Optimal Trajectories in 90°-turn Maneuver*

In what follows we present an in-depth analysis of the resulting time-optimal maneuvers for the 90°-turn. First, the computed time-optimal trajectories are explained, followed by four sections discussing different aspects of the maneuver; the global vehicle paths, the vehicle model variables, the global tire forces, and how the available tire forces are used for the particular maneuvers.

The vehicle start position was set to $(X_{p,0}, Y_{p,0}) = (37.5, 0)$ m, which is in the lower right corner in Figure 6, and the vehicle was aligned with the road direction, $\psi_0 = \pi/2$. The target vehicle position was set to $(X_{p,t_f}, Y_{p,t_f}) = (0, 37.5)$ m, where the vehicle heading should be in the road direction, $\psi_{t_f} = \pi$. Figure 7 displays the computed trajectories for the time-optimal maneuvers for the different chassis and tire model configurations in the 90°-turn. In the figure, v is the norm of the vehicle velocity vector, given by

$$v = \sqrt{v_x^2 + v_y^2},$$

and β is the body-slip angle defined as

$$\beta = \arctan\left(\frac{v_y}{v_x}\right).$$

Figure 8 shows the global forces F_X and F_Y. In addition, the yaw moment M_Z generated from the tire forces, that is, the moment about an axis orthogonal to the road, is visualized. These quantities are displayed as function of the driven distance s to enable comparison of the results for the different model configurations. Figures 9 and 10 show the Force-Slip (FS)-diagrams for ST with WF and DT with FE, respectively. The combination of longitudinal and lateral slip in the time-optimal solution is plotted on the surface; this gives an effective presentation of the solution. Moreover, Table 4 provides the execution times t_f for the maneuver with

Table 4. Time for executing the maneuver with each model configuration in the 90°-turn.

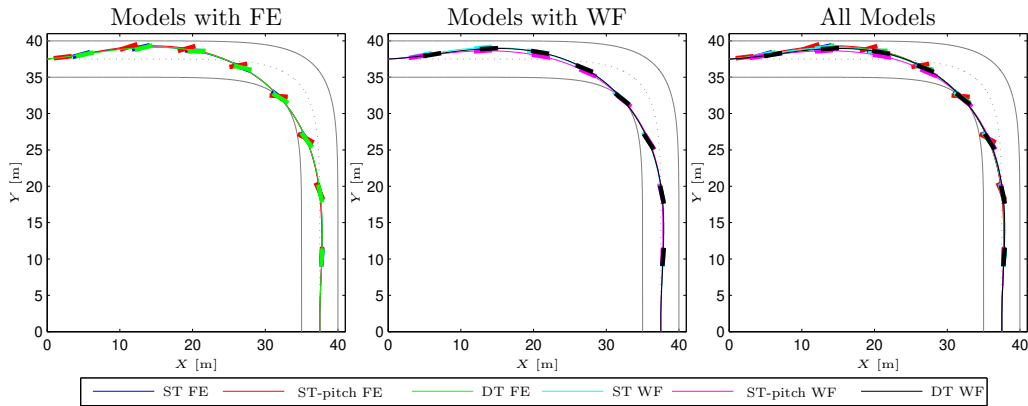| Model	Maneuver Execution Time
ST FE	4.28 s
ST WF	4.28 s
ST-pitch FE	4.12 s
ST-pitch WF	4.21 s
DT FE	4.30 s
DT WF	4.35 s

Figure 6.   Time-optimal geometric trajectories in the 90°-turn obtained for the respective model configuration. The colored bars represent the vehicle heading every half second.

the respective model configuration. The execution times vary approximately 5% at most, which occurs between the ST-pitch model with FE tire model and DT with WF tire model. It is noticeable that ST-pitch and DT exhibit larger discrepancies in execution times for the respective tire model than ST. This is most certainly a result of the load transfer incorporated in the former models, which results in significant variations in the normal load on the wheels during the maneuver. No significant trend in the execution times is observed with regard to chassis model. However, the friction ellipse seems to result in shorter execution times for ST-pitch and DT. This is because the resulting force for the friction ellipse is always larger than that for the weighting functions when combined slip is present, see Figure 4. In this maneuver combined slip is developed; hence, the friction ellipse results in larger forces and thus increased acceleration and deceleration.

5.3.1.   Geometric Trajectories

The geometric trajectories shown in Figure 6 are similar from a qualitative perspective. The largest discrepancies of the geometric trajectories occur between ST-pitch with FE and ST-pitch with WF during the exit phase, and are approximately 15% of the road width. It is interesting to note that the two ST-pitch configurations result in different strategies when exiting the turn; ST-pitch with WF results in the most narrow curve-taking, whereas ST-pitch with FE results in the most wide. However, irrespective of the tire model, the differences between the chassis models ST and DT are minor throughout the maneuver. Moreover, the geometric paths are virtually indistinguishable for the FE model configurations (even though the slip behavior is significantly different) but exhibit more variation for the WF tire models. It is plausible that this is a result of the difference in the tire force predicted by the respective model for combined slip; for the FE model, approximately the same tire force is obtained for different slip combinations. This is not the case for WF, where the tire force rapidly decreases for increasing slip quantities, and hence
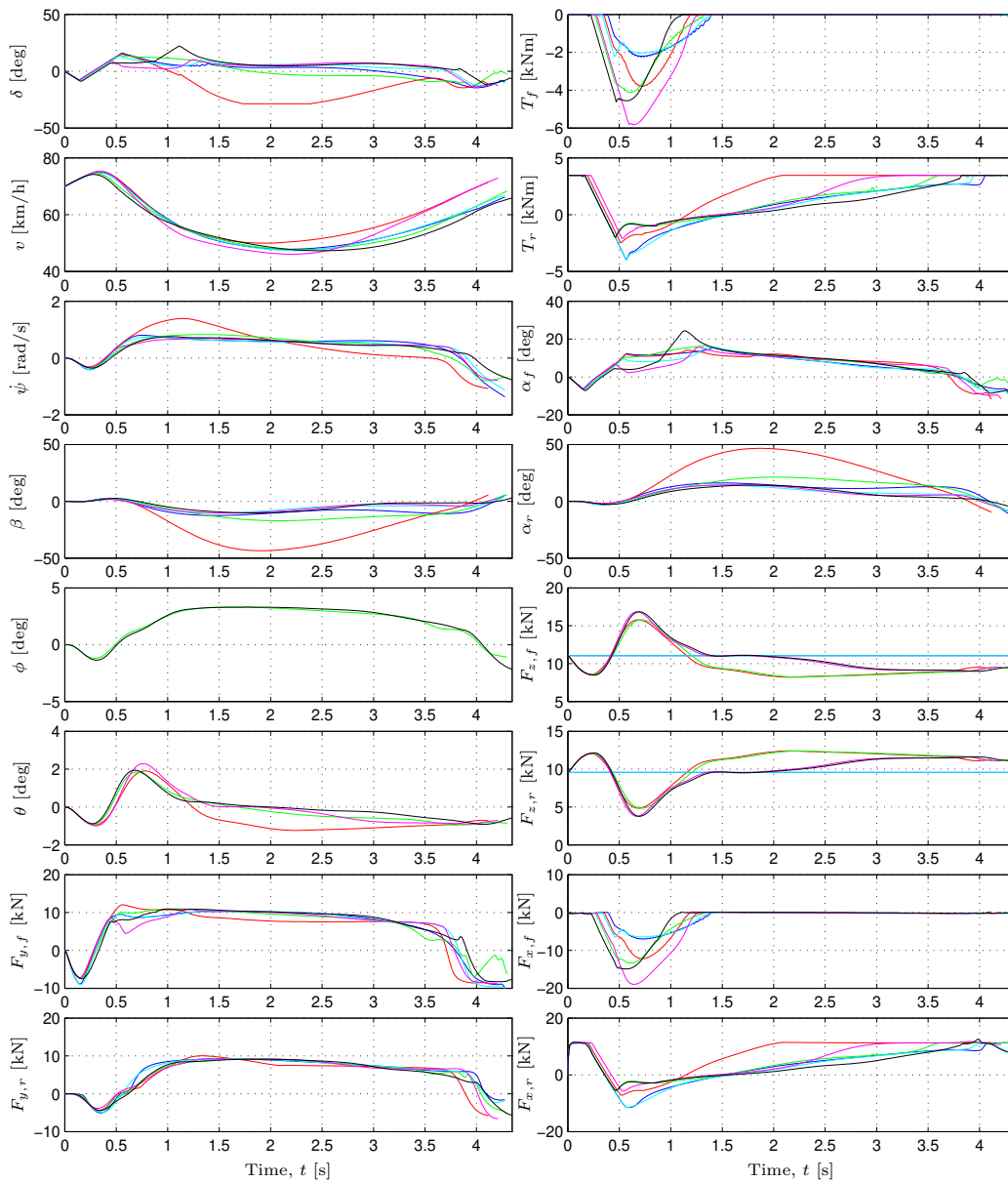
Figure 7.   Time-optimal solutions obtained for the 90°-turn, with the respective model configuration. Same colors as in Figure 6. For easier comparison F_x, F_y, T_f, and T_r have been lumped together for the DT models, yielding one longitudinal force, one lateral force, and one torque per axle. In addition, the lateral slip angles are visualized as the mean for the respective axle.
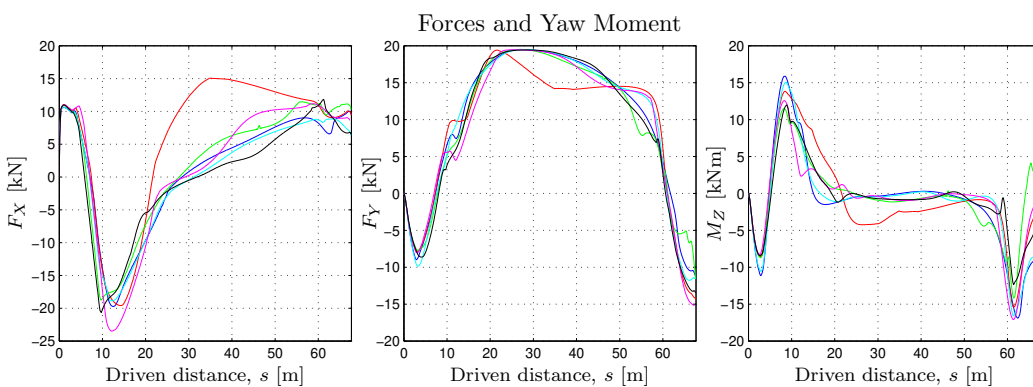
Forces and Yaw Moment

Figure 8.   Longitudinal force F_X, lateral force F_Y, and yaw moment M_Z, developed by the tires in the 90°-turn, illustrated as functions of the driven distance s. Same colors as in Figure 6.

the load transfer imposes requirements on the optimal path in the curve taking.

5.3.2.   *Trajectories of the Model Variables*

The first observation when investigating the optimal trajectories for the model variables in Figure 7 closer is that the solution obtained for ST-pitch with FE has a completely different behavior than the solutions obtained for the other model configurations. In particular, the slip behavior is much more excessive with this model configuration, which can be observed in the plots for β (peaking at a significant angle of 44°) and α_r. The observed slip behavior is also consistent with the steering angle δ that is computed, where the constraints on the angle are active for a short period around $t = 2$ s. A plausible explanation for this is that the longitudinal load transfer in combination with the characteristics of FE (compare FE and WF in Figure 4) leads to that the largest forces are attained when the vehicle both accelerates and slides. It could also be argued that the longitudinal force is used in the curve for centripetal acceleration, since the friction coefficient in the longitudinal direction is larger than in the lateral direction. For DT, however, heavy centripetal acceleration implies lateral load transfer, resulting in less available tire force for the inner wheels, thus, limiting the driving/braking effort if wheel spin/lock should be avoided. Disregarding the solution for ST-pitch with FE and considering all the remaining model configurations, the solutions are similar for several variables, being ϕ, θ, $\dot{\psi}$, and β.

Investigating the optimal vehicle trajectories further from a qualitative perspective, Figure 7 shows that the different models result in characteristics that are similar in several aspects. Prior to turning towards the corner, all solutions exhibit a slight rightward maneuvering while accelerating. This is followed by a braking phase, where both the front and the rear wheels are used. Initially in the braking phase, a significant braking torque is applied, which is gradually reducing as the vehicle approaches the turn, see T_f and T_r in Figure 7. Larger lateral forces are generated in the turn. Half-way through the turn, at $t \approx 2$ s, all solutions generate an increasing driving torque, which accelerates the vehicle out of the turn. In the final stage when exiting the turn, all solutions utilize maximum driving torque.

It can be observed that the steer angle varies considerably between the models. At $t \approx 0.7$ s, a smaller δ is obtained for the ST-pitch and DT models with WF for tire modeling, than for the remaining model configurations. For the ST-pitch and DT models with WF, the longitudinal load transfer is utilized to achieve a strategy with more emphasis on braking when entering the turn, with the lateral force being slightly smaller. Hence, a lower δ is natural. Shortly after, approximately at $t = 0.8$–1.2 s, the steer angle increases sharply in the solutions for the ST-pitch and DT models with WF for tire modeling. The effect is clearly visible for DT in the front slip angle in Figure 7. This behavior is not observed for the corresponding models with FE for tire modeling. Given the resulting forces developed at the front wheels at this time there exist two different strategies to achieve the observed behavior: Either by utilizing front wheel braking together with a moderate steering angle, or by only applying a large steer angle and achieve the longitudinal contribution from $F_{y,f} \sin(\delta)$ solely. The latter seems to be what is utilized for ST-pitch and DT with WF.

5.3.3.   *Tire Forces*

The forces that are developed by the tires, displayed in Figure 8, mirror the behavior observed in the internal model variables and geometric trajectory plots; the ST-pitch model with FE exhibits largest discrepancies. Considering the remaining configurations, F_Y and M_Z are similar from a qualitative perspective. The solutions exhibit quantitative differences in the magnitude of M_Z during the initial and exit
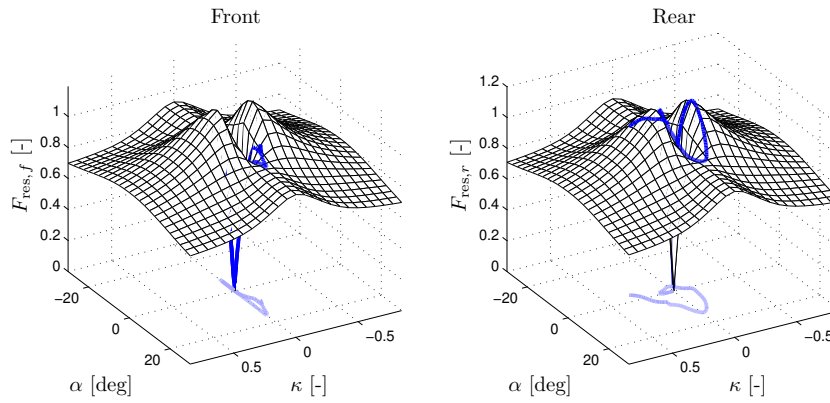
Figure 9. Resultant normalized tire forces for ST with WF tire modeling in the 90°-turn.

phases of the maneuver. This observation is also in agreement with the tire force plots in Figure 7. There are larger numerical discrepancies in F_X, at least during shorter periods of the maneuver.

The most prominent differences between the solutions appear, not unexpectedly, for the control inputs and variables closely coupled to the longitudinal dynamics of the vehicle, such as T_f, T_r, and v in Figure 7, and F_X in Figure 8. Comparing the ST models with the DT chassis models, the double-track models reduce front-wheel braking slightly earlier, see T_f in Figure 7. This is probably a consequence of T_f being equally distributed between the front wheels for the double-track models. Thus, when braking while cornering, the inner wheels will have less load and thus risk to lock up for large braking torques. Similarly, during the exit phase where lateral load-transfer still is present, a too large driving torque will spin out the inner rear-wheel. Therefore, a smaller driving torque is applied in the solution for DT compared with the optimal solutions for the ST-pitch chassis models in particular.

5.3.4. *Force-Slip Diagrams*

The Force-Slip (FS)-diagrams displayed in Figures 9 and 10 for the ST chassis model with WF and for the DT chassis models with FE, respectively, provide further information on the maneuver execution. These plots display slightly different slip characteristics for the considered model configurations. For ST, the solver chooses a control strategy such that pure slip is favored, especially for the front wheel. The DT model, having dynamically varying normal forces on the wheels, naturally exhibits different slip trajectories for the left and right wheels. From the FS-diagrams it is also clear that the slip on the rear wheels is more pronounced as a result of the vehicle being rear-wheel driven.

5.4. *Optimal Trajectories in Hairpin Maneuver*

In this section, the time-optimal maneuvers in the hairpin turn are presented. The analysis of the results for the hairpin maneuver is structured in the same manner as for the 90°-turn. The start position in the hairpin turn was $(X_{p,0}, Y_{p,0}) = (-5, 0)$ m for all models, and the initial and final heading angles were aligned with the road direction. Figures 11–12 show the vehicle path and the most relevant model variables for all six model configurations in the hairpin maneuver. The global forces and yaw moment are displayed in Figure 13, whereas the FS-diagrams for the DT chassis model with WF and FE are presented in Figures 14–15, respectively. Table 5 displays the maneuver execution times achieved with the different model configurations. The objective function t_f deviates approximately 0.4 s when comparing
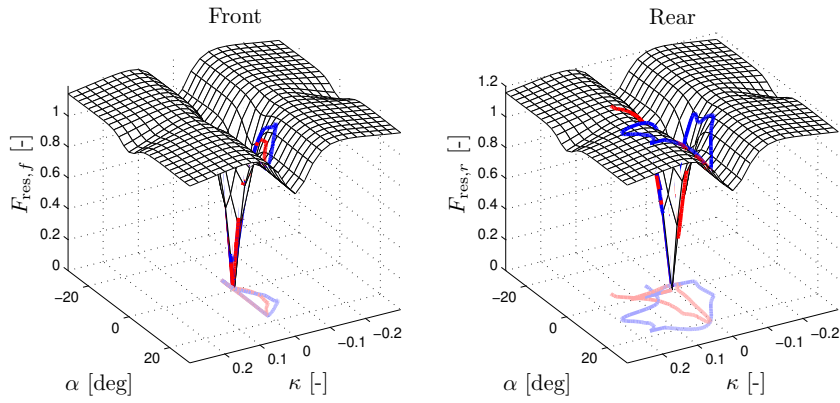
Figure 10. Resultant normalized tire forces for DT with FE tire modeling in the 90°-turn (blue – left wheel, red – right wheel).

Table 5. Time for executing the maneuver with each model configuration in the hairpin turn.

Model	Maneuver Execution Time
ST FE	8.47 s
ST WF	8.49 s
ST-pitch FE	8.19 s
ST-pitch WF	8.32 s
DT FE	8.48 s
DT WF	8.61 s

all six model configurations, corresponding to a 5% difference at most. The models with roll and/or pitch dynamics show the largest differences for the respective tire model, which is caused by that these additional dynamics lead to large wheel load variations during the maneuver. Similarly as for the 90°-turn, the models using FE for tire modeling have shortest execution times. This is because FE leads to larger resulting forces than WF for combined slip, as seen in Figure 4. With load transfer, this difference is even more pronounced. The execution times for ST-pitch is shorter than for the other models. The reason is that ST-pitch, as does DT, benefits from the longitudinal load transfer when accelerating. However, ST-pitch does not take roll dynamics into account, whereas a high cornering velocity will result in lateral load transfer caused by the roll dynamics in DT. This leads to reduced loads on the inner wheels for the double-track models, which is the same phenomenon as observed in the 90°-turn. Hence, it follows that the execution times will be shorter for ST-pitch than for both ST and DT.

5.4.1.   Geometric Trajectories

From Figure 11 we see that the geometric paths are qualitatively pairwise equal. For example, the paths for the ST models are rather symmetric in shape. The paths for the ST-pitch and DT models are asymmetric, with the ST-pitch models taking a wide exit out of the turn, and opposite for the DT models. The results seem to indicate that the qualitative behavior is more dependent on the chassis model than the tire model. However, considering the similarity of the obtained paths for the FE tire model and the differences in the paths for the WF models (in direct analogy with the results obtained in the 90°-turn), it is clear that the modeling of the tire forces for large combined slip values are important for the optimal geometric path.

June 23, 2014   13:52   Vehicle System Dynamics   journal˙vsd
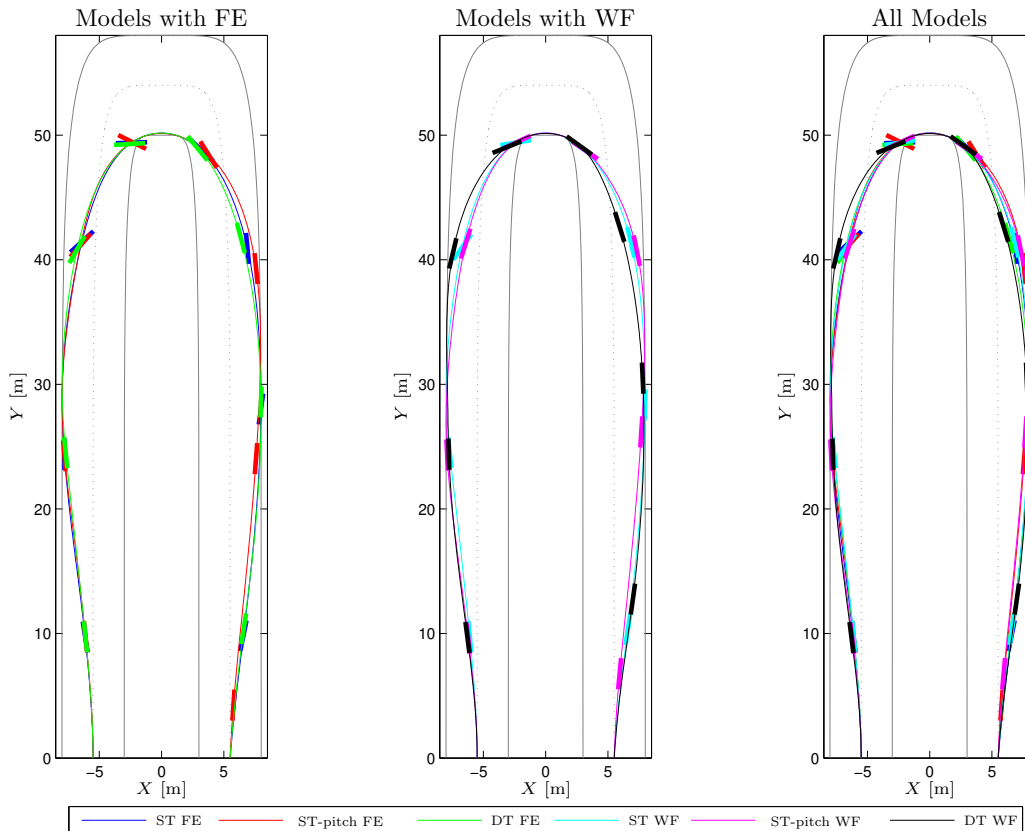
Vehicle System Dynamics   23

Figure 11.   Time-optimal geometric trajectories obtained for the hairpin turn, with the respective model configuration. The colored bars represent the vehicle heading every second.

5.4.2.   Trajectories of the Model Variables

The trajectories in Figure 12 show that all models have similarities in terms of internal variables: The vehicle starts with giving full driving torque while turning to allow for wider curve taking. When entering the curve the vehicle starts to brake with all wheels, which it does approximately until reaching the half-way point. Furthermore, all models give rise to vehicle slip. The longitudinal forces and thus also the velocities are also similar in size and shape. However, there are also fundamental differences between the models. Inspecting the body-slip angle, we see that the models with FE have significantly larger slip for the same chassis models, where, for example, β for ST-pitch peaks at approximately 60°. As mentioned previously, the reason for that FE gives larger slip is that the resulting force for FE is higher than that of WF for combined slip. These differences are coupled to the respective steer angles; δ for ST-pitch with FE is at its upper limit for approximately 1 s. For DT, and to some extent ST-pitch, with WF, there is an abrupt change in δ when reaching the leftmost part of the maneuver, at around 2 s. As discussed before, WF results in smaller forces than FE for combined slip. These forces become even smaller for the wheels on the rear axle (especially the rear inner wheel for DT) with longitudinal and/or lateral load transfer, since there will be normal-load variations when cornering and/or braking. Thus the total decelerating force will be smaller. One way to suppress this is to achieve α_f, α_r that are closer to zero, which can be achieved by the mentioned abrupt change in δ. Neither DT nor ST-pitch with FE exhibit this behavior, and it is interesting to note that the overall behavior of DT with FE is similar to the ST models in many variables.
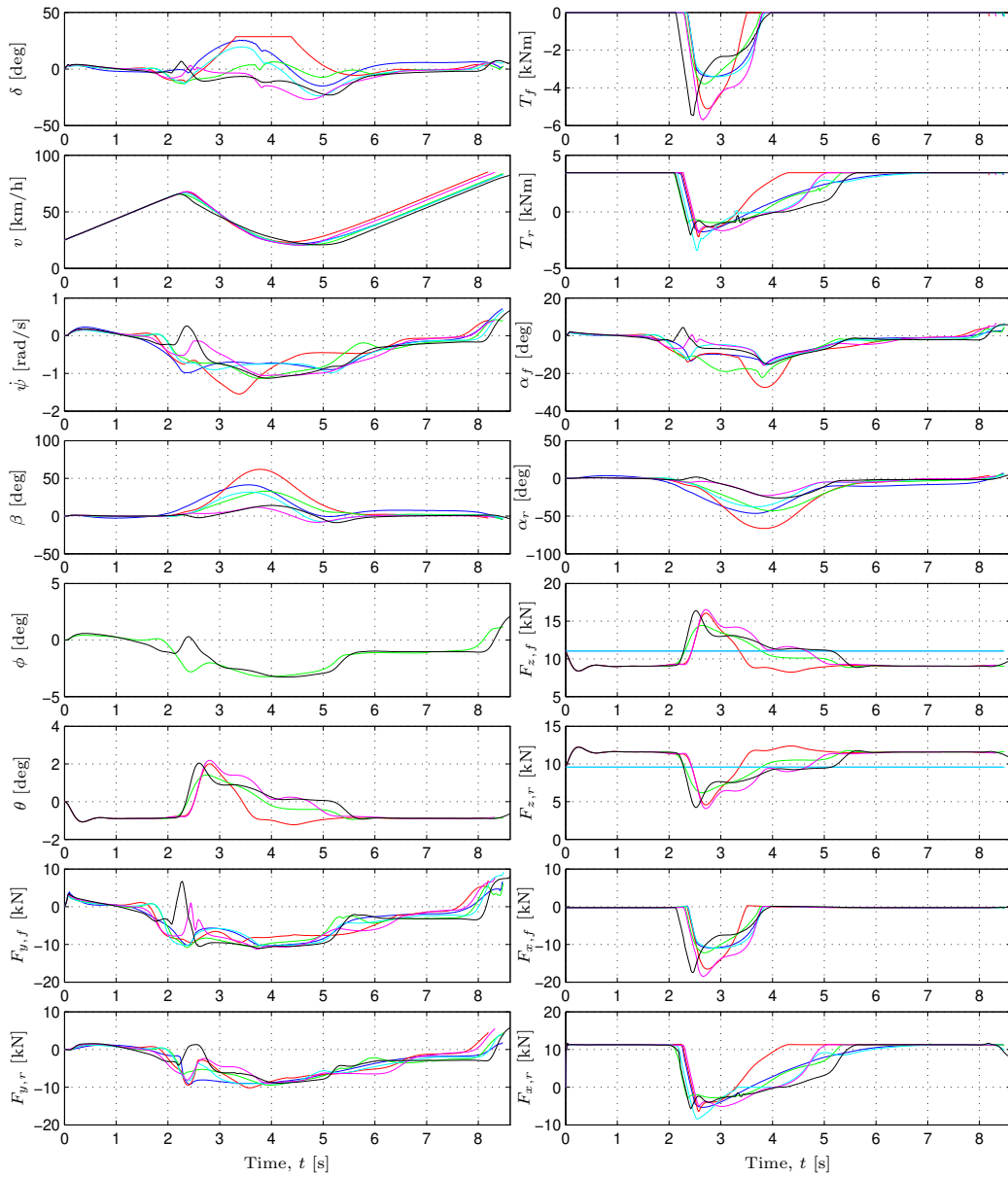
Figure 12.   Time-optimal solutions obtained for the hairpin turn, with the respective model configuration. For DT, the total forces and torques on each axle are shown. In addition, the lateral slip angles are visualized as the mean for the respective axle. Same colors as in Figure 11.
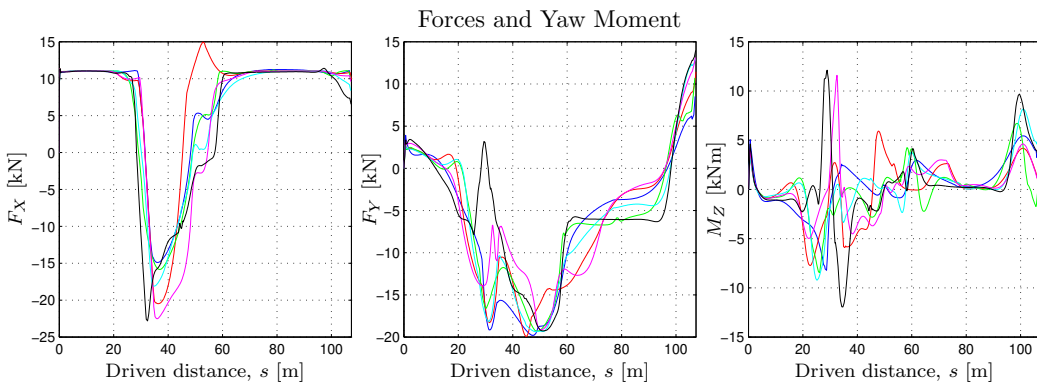

Figure 13.   Longitudinal force F_X, lateral force F_Y, and yaw moment M_Z, developed by the tires in the hairpin turn, illustrated as functions of the driven distance s. Same colors as in Figure 11.
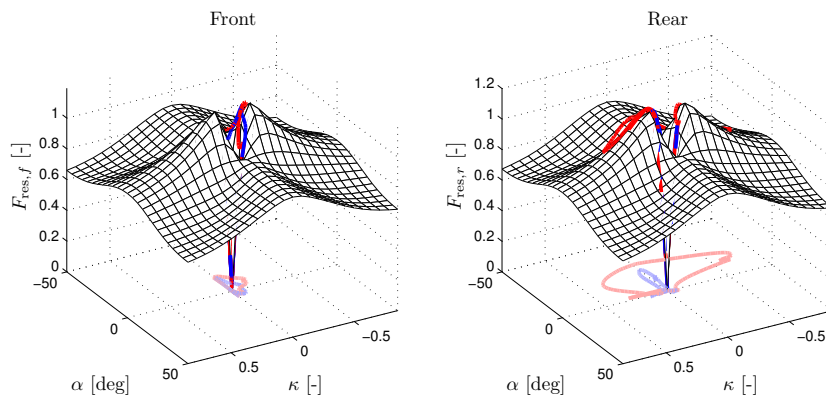
Figure 14.   Resultant tire forces for DT with WF tire modeling in the hairpin maneuver (blue – left wheel, red – right wheel).

5.4.3.   Tire Forces

Figure 13 shows the sum of the longitudinal and lateral tire-forces resolved in the road-surface plane as functions of the driven distance. In addition, the yaw moment M_Z generated from the tire forces is visualized. The qualitative behavior in the longitudinal forces exhibits similarities for all models, except for ST-pitch with FE. The behavior of the lateral forces is also rather similar, even though numerical differences occur. A significant difference is the peak in the lateral force that occurs for DT with WF approximately between $25 < s < 35$ m. This discrepancy is a result of the change in δ discussed earlier. There are qualitative discrepancies between the models in M_Z, where ST-pitch with WF, DT with WF, and ST-pitch with FE are significantly different in behavior during the turn part of the maneuver. Note that also here the overall behavior for DT with FE is alike to ST in all three plots, whereas DT with WF is fundamentally different in behavior during the critical part of the maneuver (that is, when in the turn).

5.4.4.   Force-Slip Diagrams

Figures 14 and 15 show the FS-diagrams for DT with WF and FE, respectively. It is clear that larger longitudinal slip values are obtained with WF, whereas higher lateral slip is attained with FE. This observation is related to that for WF large slip values are required in order to obtain small lateral forces but for FE longitudinal slip values of 0.1–0.2 are sufficient for this purpose. In addition, since the longitudinal force does not depend on the lateral slip in the adopted FE model, in contrast to the WF model, the observed behavior is expected. With FE, changes in the resulting force seem to have a tendency of moving in orthogonal directions; when altering κ, the lateral slip α hardly changes, and vice versa. However, this is partly a result of that the wheel-torque constraints have been reached (especially for negative slip ratios), and not solely attributes of the FE tire model.

6.   Discussion and Conclusions

The time-optimal trajectories in three different time-critical maneuvers were determined for several vehicle-model configurations. Two of them, the 90°-turn and the hairpin turn, were investigated in detail in this paper. The double lane-change maneuver provided results that lead to similar conclusions as those for the two reported maneuvers, and this is an important verification that the developed platform can handle a variety of situations relevant for vehicle safety systems. It should also be noted that we have used the same methodology for investigation of the in-
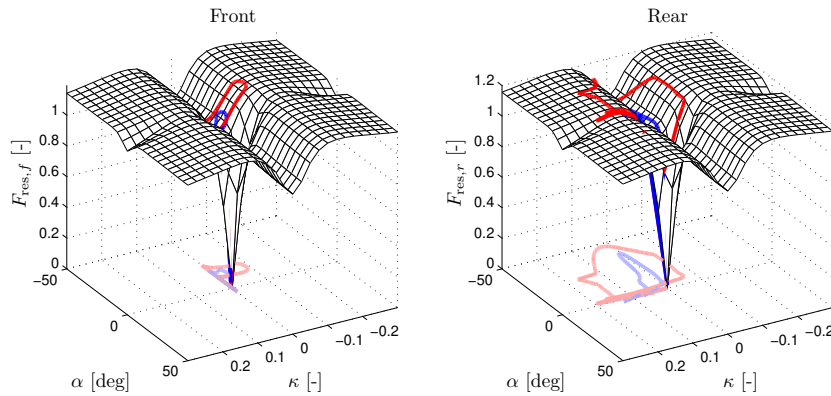
Figure 15.   Resultant tire forces for DT with FE tire modeling in the hairpin maneuver (blue – left wheel, red – right wheel). In contrast to Figure 14, the FE tire model results in smaller longitudinal slip but larger lateral slip. That is, the desired forces are achieved by sliding rather than spinning up or locking the wheels.

fluence on the road surface on the optimal maneuver, see [29]. Thus, we believe that the platform is an effective tool for investigation of optimal vehicle maneuvers and subsequent trajectory generation. Moreover, as, for example, Table 1 shows, it gives valuable insight into the balance between model detail and computational complexity, which is important for development toward online solutions for optimal vehicle safety systems.

The obtained results provide a solid basis for discussion of vehicle-model behavior in time-critical situations. Several interesting properties were found: The differences in behavior for M_Z between the investigated models is interesting because this variable is often used as a high-level input in safety systems, such as in yaw-rate controllers and rollover-prevention systems [16, 17, 26, 47]. Thus, it seems that the choice of models can potentially lead to fundamentally different control strategies, where, for example, whether to use WF instead of FE with the DT chassis model seems crucial. The characteristics of the two tire models are fundamentally different. The WF model results in much smaller forces for combined slip compared with when only one of the slip quantities is nonzero. For the FE model, however, the largest forces are attained for combined slip. It is hard to verify which of the models that are most suitable to use for trajectory generation in extreme maneuvering. The WF model has been experimentally verified for normal driving conditions on specific road surfaces. However, for large combined slip, we find it hard to explain why the resulting force should be significantly smaller than for pure longitudinal or lateral slip of similar magnitude. Similarly, it is not reasonable that the largest forces should be attained for combined slip, which the FE model predicts as a result of that the longitudinal force is not affected by the lateral slip. Whether to use ST or DT has impact on the employed control strategy. The intuitively obvious choice would be to use DT, because it is a more advanced model. However, the optimal solutions that are obtained indicate that the models with load transfer are highly dependent on the choice of tire model, where the different characteristics for combined slip has large impact on the solutions. Thus, it is possible that certain combinations of chassis and tire models are inappropriate and lead to nonphysical behavior, as surveyed in [4] and discussed in Section 1.

Maneuvering techniques employed by expert drivers in narrow turns, similar to the hairpin turn, on dry asphalt generally exhibit minor body slip even though individual variations occur. This is, for example, illustrated with measurement data for a rear-wheel driven vehicle in [12], a front-wheel driven vehicle in [20], and for an all-wheel driven vehicle in [10]. If assuming that the driving techniques with smaller body slip are close to time-optimal, it can be argued that the results obtained

with ST-pitch FE, resulting in significant body slip, are not in agreement with reality. Based on this observation, and on the comment regarding inappropriate combinations in the previous paragraph, the ST-pitch models are not considered in the following discussion about the physical consequences in practice.

Considering that the computed time-optimal maneuvers result in at-the-limit behavior of the vehicle, we believe that the observations made in this paper have important implications for future safety systems. The solution behavior is similar in several key aspects for both maneuvers, as observed in Figures 7 and 12; for example, variables traditionally used for detecting loss of maneuvering stability, such as the yaw rate, the slip angle, and the roll angle, only show minor discrepancies. The input torques differ significantly during parts of the maneuver. In the 90°-turn, however, the overall lateral forces and yaw moments generated by the tires (see Figure 8) for the considered models have similar characteristics from a qualitative perspective, but with numerical differences in between for certain model configurations. The discrepancies do not have much impact on the other model variables. Moreover, model parameters such as the friction coefficients, vehicle mass, and tire parameters are uncertain. Hence, safety bounds on supervisory variables have to be set conservatively, for example resulting in early braking in order to surely avoid impact, and the model deviations occurring for low-order models will be suppressed in an online implementation with feedback. The observations are important, because they imply that variables traditionally considered as high-level inputs in safety systems, such as M_Z, may be generated by optimization using models of low complexity (such as the single-track model). These high-level inputs can then be utilized as inputs to a low-level optimizer, which benefit more from complex road interaction models for distributing the desired torque to the respective wheel. This fact, together with the increased amount of sensor data and computational power available in modern road vehicles, opens up for the use of simplistic models when designing the online optimization-based safety systems of tomorrow.

References

[1] R. Isermann *Fahrdynamik-Regelung: Modellbildung, Fahrerassistenzsysteme, Mechatronik*, Vieweg-Verlag, Wiesbaden, Germany, 2006.
[2] K. Liebemann, K. Meder, J. Schuh, and G. Nenninger, *Safety and Performance Enhancement: The Bosch Electronic Stability Control*, (2005), Paper Number 05-0471m, Robert Bosch GmbH, Germany.
[3] J. Funke, P. Theodosis, R. Hindiyeh, G. Stanek, K. Kritatakirana, C. Gerdes, D. Langer, M. Hernandez, B. Muller-Bessler, and B. Huhnke, *Up to the limits: Autonomous Audi TTS*, in *Proc. IEEE Intelligent Vehicles Symp.*, Alcalá de Henares, Spain, 2012, pp. 541–547.
[4] R.S. Sharp and H. Peng, *Vehicle dynamics applications of optimal control theory*, Vehicle System Dynamics 49 (2011), pp. 1073–1111.
[5] H.B. Pacejka *Tire and Vehicle Dynamics*, 2 Butterworth-Heinemann, Oxford, United Kingdom, 2006.
[6] C. Carlson and J. Gerdes, *Consistent nonlinear estimation of longitudinal tire stiffness and effective radius*, IEEE Trans. Control Syst. Technol. 13 (2005), pp. 1010–1020.
[7] F. Braghin, F. Cheli, and E. Sabbioni, *Environmental effects on Pacejka's scaling factors*, Vehicle System Dynamics 44 (2006), pp. 547–568.
[8] I. Chakraborty, P. Tsiotras, and R.S. Diaz, *Time-optimal vehicle posture control to mitigate unavoidable collisions using conventional control inputs*, in *Proc. Am. Control Conf. (ACC)*, Washington, DC, 2013, pp. 2165–2170.
[9] E. Esmailzadeh, A. Goodarzi, and G. Vossoughi, *Optimal yaw moment control law for improved vehicle handling*, Mechatronics 13 (2003), pp. 659–675.
[10] J. Yi, J. Li, J. Lu, and Z. Liu, *On the Stability and Agility of Aggressive Vehicle Maneuvers: A Pendulum-Turn Maneuver Example*, IEEE Trans. Control Syst. Technol. 20 (2012), pp. 663–676.
[11] P. Dingle and L. Guzzella, *Optimal emergency maneuvers on highways for passenger vehicles with two- and four-wheel active steering*, in *Proc. Am. Control Conf.*, Baltimore, MD, 2010, pp. 5374–5381.
[12] E. Velenis, *FWD Vehicle Drifting Control: The Handbrake-Cornering Technique*, in *Proc. IEEE Conf. Decision and Control*, Orlando, FL, 2011, pp. 3258–3263.
[13] J.P. Timings and D.J. Cole, *Minimum Maneuver Time Calculation Using Convex Optimization*, ASME J. Dynamic Systems, Measurement, and Control 135 (2013), pp. 031015–1–031015–9.
[14] P. Sundström, M. Jonasson, J. Andreasson, A. Stensson Trigell, and B. Jacobsson, *Path and control optimisation for over-actuated vehicles in two safety-critical maneuvers*, in *Proc. 10th Int. Symp. Advanced Vehicle Control*, Loughborough, United Kingdom, 2010.

[15] J. Andreasson, *Enhancing active safety by extending controllability—How much can be gained?*, in *Proc. IEEE Intelligent Vehicles Symp.*, Xi'an, Shaanxi, China, 2009, pp. 658–662.

[16] P. Tøndel and T. Johansen, *Control allocation for yaw stabilization in automotive vehicles using multiparametric nonlinear programming*, in *Proc. Am. Control Conf.*, Portland, OR, 2005, pp. 453–458.

[17] B. Schofield, *Model-Based Vehicle Dynamics Control for Active Safety*, Ph.D. Thesis ISRN LUTFD2/TFRT--1083--SE, Department of Automatic Control, Lund University, Sweden, 2008.

[18] I. Chakraborty, P. Tsiotras, and J. Lu, *Vehicle Posture Control through Aggressive Maneuvering for Mitigation of T-bone Collisions*, in *Proc. IEEE Conf. Decision and Control*, Orlando, FL, 2011, pp. 3264–3269.

[19] E. Velenis and P. Tsiotras, *Minimum Time vs. Maximum Exit Velocity Path Optimization During Cornering*, in *Proc. IEEE Int. Symp. Industrial Electronics*, Dubrovnik, Croatia, 2005, pp. 355–360.

[20] D. Tavernini, M. Massaro, E. Velenis, D.I. Katzourakis, and R. Lot, *Minimum Time Cornering: The Effect of Road Surface and Car Transmission Layout*, Vehicle System Dynamics 51 (2013), pp. 1533–1547.

[21] Z. Shiller and S. Sundar, *Emergency lane-change maneuvers of autonomous vehicles*, ASME J. Dynamic Systems, Measurement, and Control 120 (1998), pp. 37–44.

[22] D.P. Kelly and R.S. Sharp, *Time-optimal control of the race car: a numerical method to emulate the ideal driver*, Vehicle System Dynamics 48 (2010), pp. 1461–1474.

[23] D. Casanova, *On minimum time vehicle manoeuvring: The theoretical optimal lap*, Ph.D. Thesis, Cranfield University, United Kingdom, 2000.

[24] S. Anderson, S. Peters, T. Pilutti, and K. Iagnemma, *An Optimal-Control-Based Framework for Trajectory Planning, Threat Assessment, and Semi-Autonomous Control of Passenger Vehicles in Hazard Avoidance Scenarios*, Int. J. Vehicle Autonomous Systems 8 (2010), pp. 190–216.

[25] S. Anderson, S. Karumanchi, and K. Iagnemma, *Constraint-Based Planning and Control for Safe, Semi-Autonomous Operation of Vehicles*, in *Proc. IEEE Intelligent Vehicles Symp.*, Alcalá de Henares, Spain, 2012, pp. 383–388.

[26] J. Tjønnås and T. Johansen, *Stabilization of Automotive Vehicles Using Active Steering and Adaptive Brake Control Allocation*, IEEE Trans. Control Syst. Technol. 18 (2010), pp. 545–558.

[27] K. Berntorp, B. Olofsson, K. Lundahl, B. Bernhardsson, and L. Nielsen, *Models and Methodology for Optimal Vehicle Maneuvers Applied to a Hairpin Turn*, in *Proc. Am. Control Conf. (ACC)*, Washington, DC, 2013, pp. 2139–2146.

[28] K. Lundahl, K. Berntorp, B. Olofsson, J. Åslund, and L. Nielsen, *Studying the Influence of Roll and Pitch Dynamics in Optimal Road-Vehicle Maneuvers*, in *Proc. 23rd Int. Symp. Dynamics of Vehicles on Roads and Tracks (IAVSD)*, Qingdao, China, 2013.

[29] B. Olofsson, K. Lundahl, K. Berntorp, and L. Nielsen, *An Investigation of Optimal Vehicle Maneuvers for Different Road Conditions*, in *Proc. 7th IFAC Symp. Advances in Automotive Control*, Tokyo, Japan, 2013, pp. 66–71.

[30] K. Lundahl, J. Åslund, and L. Nielsen, *Vehicle Dynamics Platform, Experiments, and Modeling Aiming at Critical Maneuver Handling*, Technical Report LiTH-R-3064, Department of Electrical Engineering, Linköpings Universitet, SE-581 83 Linköping, Sweden, 2013.

[31] K. Berntorp, *Particle Filtering and Optimal Control for Vehicles and Robots*, Department of Automatic Control, Lund University, Sweden, 2014.

[32] ———, *Derivation of a Six Degrees-of-Freedom Ground-Vehicle Model for Automotive Applications*, Technical Report ISRN LUTFD2/TFRT--7627--SE, Department of Automatic Control, Lund University, Sweden, 2013.

[33] E. Schindler *Fahrdynamik: Grundlagen Des Lenkverhaltens Und Ihre Anwendung Für Fahrzeugregelsysteme*, Expert-Verlag, Renningen, Germany, 2007.

[34] U. Kiencke and L. Nielsen *Automotive Control Systems—For Engine, Driveline and Vehicle*, 2 Springer-Verlag, Berlin Heidelberg, Germany, 2005.

[35] R. Rajamani *Vehicle Dynamics and Control*, Springer-Verlag, Berlin Heidelberg, Germany, 2006.

[36] J. Wong *Theory of Ground Vehicles*, John Wiley & Sons, Hoboken, NJ, 2008.

[37] Modelica Association URL: http://www.modelica.org.

[38] J. Åkesson, *Optimica—An Extension of Modelica Supporting Dynamic Optimization*, in *Proc. 6th Int. Modelica Conf.*, Bielefeld, Germany, 2008, pp. 57–66.

[39] L.T. Biegler, A.M. Cervantes, and A. Wächter, *Advances in simultaneous strategies for dynamic process optimization*, Chemical Engineering Science 57 (2002), pp. 575–593.

[40] J. Åkesson, *Languages and Tools for Optimization of Large-Scale Systems*, Ph.D. Thesis ISRN LUTFD2/TFRT--1081--SE, Department of Automatic Control, Lund University, Sweden, 2007.

[41] A. Wächter and L.T. Biegler, *On the implementation of an interior-point filter line-search algorithm for large-scale nonlinear programming*, Mathematical Programming 106 (2006), pp. 25–57.

[42] J. Åkesson, K.E. Årzén, M. Gäfvert, T. Bergdahl, and H. Tummescheit, *Modeling and Optimization with Optimica and JModelica.org—Languages and Tools for Solving Large-Scale Dynamic Optimization Problems*, Computers and Chemical Engineering 34 (2010), pp. 1737–1749.

[43] JModelica.org URL: http://www.jmodelica.org.

[44] J. Dennis and R. Schnabel *Numerical Methods for Unconstrained Optimization and Nonlinear Equations*, Classics in Applied Mathematics, Society for Industrial and Applied Mathematics, 1983.

[45] A. Griewank, *Evaluating Derivatives: Principles and Techniques of Algorithmic Differentiation*, Frontiers in Applied Mathematics, SIAM 19 (2000).

[46] ISO 3888-2:2011 *Passenger cars—Test track for a severe lane-change manoeuvre—Part 2: Obstacle avoidance*, International Organization for Standardization, Geneva, Switzerland, 2011.

[47] K. Berntorp, *ESP for Suppression of Jackknifing in an Articulated Bus*, Master's Thesis ISRN LUTFD2/TFRT--5831--SE, Department of Automatic Control, Lund University, Sweden, 2008.